Resolving the stratification discrepancy of turbulent natural convection in differentially heated air-filled cavities. Part II: end wall effects

Anne Sergent, Patrice Joubert, Shihe Xin, Patrick Le Quéré

▶ To cite this version:

Resolving the stratification discrepancy of turbulent natural convection in differentially heated air-filled cavities
Part II: End walls effects

A. Sergent [a,b,*] , P. Joubert [c], S. Xin [d], P. Le Quéré [a]

[a] *CNRS, LIMSI, BP 133, 91403 Orsay, France*
[b] *UPMC Univ Paris 06, F-75005, Paris, France*
[c] *LEPTIAB, Université de La Rochelle,17042 La Rochelle cedex 1, France*
[d] *CETHIL, CNRS/INSA-Lyon/UCBL, 69621 Villeurbanne cedex, France*

* Corresponding author.
  Email address: `sergent@limsi.fr` (A. Sergent).

Abstract:

This paper provides an explanation for the discrepancy in the central thermal stratification long observed between experimental and numerical studies of natural convection at high Rayleigh number in air-filled differentially heated cavities. The turbulent natural convection flow ($Ra_H = 1.5 \times 10^9$) is investigated by means of large eddy simulations, which are first validated in comparison with the spectral simulations data presented in the first part of this paper (Sergent et al., 2010). Three sets of simulations are performed in configurations of increasing consideration of the experimental temperature distributions at the end walls. Results show that the complete set of experimental temperature distribution is needed to recover full agreement between numerical and experimental results. In particular, the thermal boundary conditions on the front and rear walls are found to be the key ingredient to obtain a good agreement. In the third part of this paper it is shown that this temperature distribution results from a complete 3D convection-conduction-radiation coupling at the cavity walls (Xin et al., 2010).

Keywords: *natural convection, differentially heated cavity, large eddy simulation, turbulence*

1   Introduction

A canonical configuration of natural convection flow is a parallelepipedic cavity, where two opposite vertical walls are differentially heated. This flow has been extensively studied in the past, but has regained much attention when new detailed experimental data have been published for parameter values corresponding to a weakly turbulent regime (Tian and Karayiannis, 2000; Betts and Bokhari, 2000; Ampofo and Karayiannis, 2003). Simultaneously the improved computing capabilities have enabled the use of realistic meshes for the simulation of flows which combine separated recirculating areas and thin vertical boundary layers. This is the reason why this configuration remains a challenging case for analysing numerical algorithms dedicated to Navier-Stokes equations (for instance, Wakashima and Saitoh (2004); Feldman and Gelfgat (2009)) or for providing benchmark solutions (Tric et al., 2000) as well as for testing turbulence models of Reynolds Averaged Navier-Stokes (RANS) or Large Eddy Simulation (LES) approaches (Peng and Davidson, 2001; Sergent et al., 2003; Kenjeres et al., 2005; Knopp et al., 2005; Baraghi and Davidson, 2007; Choi and Kim, 2008).

In the early nineties, the concomitant agreement of the 2D turbulent RANS reference solution and Paolucci's DNS solution with available experimental results could lead one to conclude that 2D RANS modeling embodied all the 3D physical phenomena responsible for the weak stratification in the experiments. In cavities of height to width aspect ratios between 1 and 5, Cheesewright et al. (1986) reported an experimental value $<S>= 0.51$ for the core stratification, whereas Mergui and Penot (1997) reported $<S>= 0.37$ and Tian and Karayiannis (2000) reported $<S>= 0.50$. More recently, Salat and Penot (2003) obtained values between $<S>= 0.375$ and 0.72, depending on the radiative properties of the cavity front and rear walls. But an important discrepancy in $<S>$ was observed between 2D DNS and LES ($<S>\sim 1$) on the one hand and experimental and RANS approaches ($<S>\sim 1/2$) on the other hand. These facts in turn cast doubt on the capability of 2D DNS to reproduce the physical aspects of natural convection flow in DHC. As experimental measurements on the cavity horizontal walls have revealed temperature distributions in clear disagreement with the numerical results obtained with adiabatic conditions, thermal boundary conditions (BC) imposed on the top and bottom walls are suspected to be at the origin of this discrepancy (Le Quéré, 1994). Unfortunately, 2D DNS performed at high Rayleigh number with BC corresponding to experimental measurements of the wall temperature or their analytical fits did not help resolving the stratification paradox (Salat et al., 2004; Sergent et al., 2010). This suggested, in accordance with Fusegi and Hyun (1994), that realistic thermal BC on the top and bottom walls are not the only key factors responsible for the weak vertical stratification in the experimental studies. Possible non-boussinesq effects (and variable-property fluid), or imperfect adiabatic BC on the non-isothermal walls or again end walls effects could also be responsible for the stratification discrepancy. Des lignes sur Borjini et al. (2008) sont commentées !

In the scope of the joint research program set up in order to understand the unexplained discrepancy observed on thermal stratification in the cavity core, experimental approach has been used along with 3D DNS and LES. (A new experiment (Salat et al., 2004; Salat, 2004) has been built and will be presented in Part III (Xin et al., 2010).) The DNS simulations presented in the first part of this paper (Sergent et al., 2010) show that going from Perfectly Adiabatic Cavity (PAC) to Intermediate Realistic Cavity (IRC) does improve substantially the prediction of the flow structure and of the turbulence structure within the cavity, but there is almost no effect on the thermal stratification in the cavity core. It means that considering the realistic BC only on the top and bottom walls is not enough to reproduce the experimental level of stratification. These

findings contradict the observations of Peng and Davidson (2001) on the experimental cavity of Tian and Karayiannis (2000) at $Ra = 1.58 \times 10^9$.

The above observations lead to the conclusion that, in comparison with experimental investigations, some ingredients are missing in the DNS performed and that the missing ingredients have to be brought in to reconcile the numerical and experimental results. The aim of this paper is to put in evidence that flow structure is considerably modified by the deviation from convective adiabaticity of the thermal BC on the front/rear walls and to explain how these changes modify the thermal stratification. For this purpose, two additional configurations have been defined: in order to understand the role played by the front/rear wall a periodic configuration with periodic condition in y direction is specified on the one hand and on the other hand measured temperature distributions are applied on the front and rear vertical walls in order to increase the realism of the thermal BC. Introduction of measured temperature distributions in 3D numerical simulations (LES) as Dirichlet BC needs a close interaction between numerical and experimental approaches but avoids considering numerically the full thermal coupling of conduction, convection and radiation on walls insofar as the temperature distribution results from the thermal balance at wall.

The outline of this paper is as follows. Section 2 is devoted to the physical problem of interest. In section 3, LES approach is presented together with a short description of the numerical method that is employed. In subsection 4.1 are described the investigated configurations which attempt to consider more and more the experiment characteristics. In subsection 4.2, LES methodology is validated in comparison with the DNS results of the IRC configuration. Influence of the boundary conditions in the spanwise y direction is then discussed in subsection 4.3) and improvement in predicting the thermal stratification is assessed in subsection 4.4. Final discussions will be given before the conclusions.

2   Physical Problem

A cavity of width W in the x direction, depth D in the spanwise y direction and height H in the vertical z direction is filled with air (Fig. 1). Its two opposite vertical walls in the x direction are maintained at uniform but different temperatures T_h at $x = 0$ and T_c at $x = W$.

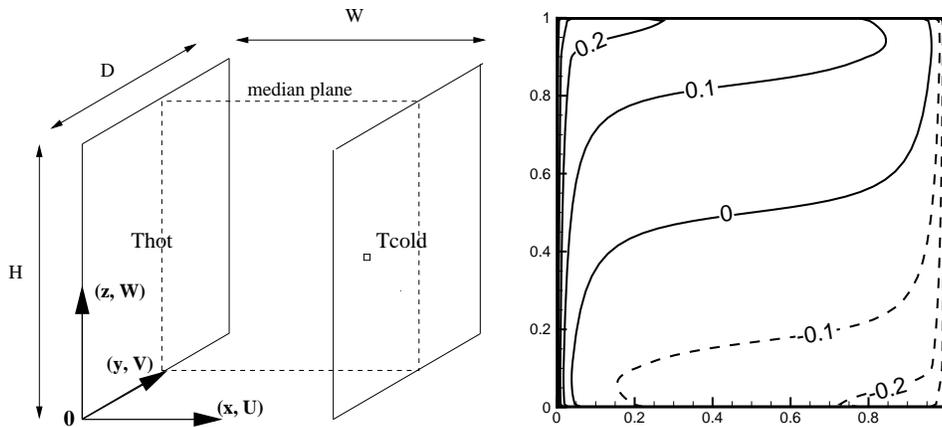The problem depends on the thermal BC on other walls and the following

Fig. 1. Geometry definition (left) and smoothed front and rear walls temperature distributions reconstructed from infrared camera measurements (Salat, 2004) (right).

dimensionless parameters: the geometrical aspect ratios ($A_x = W/H = 1$, $A_y = D/H = 0.32$, $A_z = 1$), the Prandtl number, $Pr = \nu/\alpha$ ($Pr = 0.71$ for air) and the Rayleigh number, $Ra = g\beta\Delta T H^3/\nu\alpha$ ($Ra = 1.5 \cdot 10^9$), where $\Delta T = T_h - T_c$, β is volumetric thermal expansion coefficient, g gravity acceleration, ν kinematic viscosity and α thermal diffusivity. The above values of dimensionless parameters are those of the experimental facility (Salat, 2004).

In this paper, temperature distributions independent of y and t are imposed on the top and bottom walls and they correspond to the analytical fits of the measured temperature (Salat, 2004). Depending on the investigated configuration, flow in the cavity could be either periodic in the spanwise y direction (PRC) or confined by the front/rear walls. In the latter case, the vertical front/rear walls can be thermally insulated (IRC) or maintained at time-independent temperature distributions (FRC). A complete description of the studied cases is given in section 4.1.

In terms of thermal stratification and heat transfer, time-averaged flow investigated is characterized by time-averaged vertical temperature gradient at the cavity center and different Nusselt numbers. Although they have been defined in Part I (Sergent et al., 2010), their definitions are repeated here:

- thermal stratification: $<S> = \dfrac{\partial <\theta>}{\partial z}(A_x/2, A_y/2, 0.5)$ where $<\cdot>$ denotes time averaging and $\theta = (T - T_0)/\Delta T$ is the reduced temperature with $T_0 = (T_h + T_c)/2$.
- 1D Nusselt numbers averaged along the vertical and horizontal lines

5

at the cavity mid-depth ($y = A_y/2$):

$$<\overline{Nu}_{1D,hot}> = \int_0^1 \frac{\partial <\theta>}{\partial x}(0, A_y/2, z)dz \text{ and } <\overline{Nu}_{1D,cold}> = \int_0^1 \frac{\partial <\theta>}{\partial x}(A_x, A_y/2, z)dz$$

$$<\overline{Nu}_{1D,bottom}> = \frac{1}{A_x}\int_0^{A_x} \frac{\partial <\theta>}{\partial z}(x, A_y/2, 0)dx \text{ and } <\overline{Nu}_{1D,top}> = \frac{1}{A_x}\int_0^{A_x} \frac{\partial <\theta>}{\partial z}(x, A_y/2, 1)dx$$

- 2D Nusselt numbers averaged over the vertical and horizontal walls:

$$<\overline{Nu}_{2D,hot}> = \frac{1}{A_y}\int_0^1\int_0^{A_y} \frac{\partial <\theta>}{\partial x}(0, y, z)dydz \text{ and } <\overline{Nu}_{2D,cold}> = \frac{1}{A_y}\int_0^1\int_0^{A_y} \frac{\partial <\theta>}{\partial x}(1, y, z)dydz$$

$$<\overline{Nu}_{2D,bottom}> = \frac{1}{A_x \times A_y}\int_0^{A_x}\int_0^{A_y} \frac{\partial <\theta>}{\partial z}(x, y, 0)dydx \text{ and } <\overline{Nu}_{2D,top}> =$$

$$\frac{1}{A_x \times A_y}\int_0^{A_x}\int_0^{A_y} \frac{\partial <\theta>}{\partial z}(x, y, 1)dydx$$

3 Mathematical formulations and numerical methods

3.1 Large Eddy Simulations

The governing equations for the LES of an incompressible fluid flow under Boussinesq assumption are derived by applying a convolution filter ($\overline{\cdot}$) to the unsteady momentum and energy equations. The resulting set of non-dimensional equations reads:

$$\begin{cases} \dfrac{\partial \bar{u}_i}{\partial x_i} = 0 \\ \dfrac{\partial \bar{u}_i}{\partial t} + \dfrac{\partial \bar{u}_i \bar{u}_j}{\partial x_j} = -\dfrac{\partial \bar{p}}{\partial x_i} + \dfrac{\partial}{\partial x_j}(PrRa^{-\frac{1}{2}}(\dfrac{\partial \bar{u}_i}{\partial x_j} + \dfrac{\partial \bar{u}_j}{\partial x_i})) - \dfrac{\partial \tau_{ij}}{\partial x_j} + Pr\bar{\theta}\delta_{i3} \quad (1) \\ \dfrac{\partial \bar{\theta}}{\partial t} + \dfrac{\partial \bar{\theta}\bar{u}_j}{\partial x_j} = \dfrac{\partial}{\partial x_j}(Ra^{-\frac{1}{2}}\dfrac{\partial \bar{\theta}}{\partial x_j}) - \dfrac{\partial h_j}{\partial x_j} \end{cases}$$

Equations (1) are obtained by using cavity height (H) as reference length and the convective velocity ($\alpha Ra^{1/2}/H$) as reference velocity. t denotes time, x_i the coordinates ($x_i = (x, y, z)$), $\bar{u}_i$ is the resolved velocity component in the x_i−direction ($\bar{u}_i = (\bar{u}, \bar{v}, \bar{w})$), $\bar{p}$ is the resolved pressure and $\bar{\theta}$ the filtered reduced temperature ($\theta = (\overline{T} - T_0)/\Delta T$), ranges from -0.5 on cold wall to 0.5 on the hot wall.

Therefore on the vertical active walls ($x = 0$ and $x = A_x$), temperature is specified and no-slip condition for velocity is applied. On the top/bottom

horizontal walls ($z = 0$ and $z = 1$), thermal BC are taken to be of Dirichlet type (measured distributions) and no-slip condition is also used. In the spanwise y direction, flow could be either periodic or delimited by the front/rear vertical walls ($y = 0, y = A_y$). In the former case, both temperature and velocity are periodic and in the latter case no-slip condition is applied for velocity and thermal BC are either adiabatic or of Dirichlet type. Details of the thermal BC used will be given along with the configurations studied in section 4.1. .

The effects of the subgrid scales removed by the filtering operation on the resolved quantities ($\bar{\cdot}$) is accounted for by the subgrid-scale stress (SGS) tensor τ_{ij} ($\tau_{ij} = \overline{u_i u_j} - \bar{u}_i \bar{u}_j$) and heat flux vector h_j ($h_j = \overline{\theta u_j} - \bar{\theta}\bar{u}_j$). The SGS stresses need to be modeled in terms of the resolved variables in order to solve the equations. Because only eddy-viscosity type models are considered here, the isotropic part of the SGS tensor is added to the filtered pressure, leading to the definition of a modified pressure, $\bar{p}^* = \bar{p} + \dfrac{1}{3}\tau_{ii}$. We use the subgrid model which has been previously presented in Sergent et al., 2003; Salat et al., 2004. This model, called Mixed Scale Diffusivity Model (MSDM), has been developed on the basis of the Mixed Scale Viscosity Model proposed by Sagaut et al. (1996). It uses its own time scale, independent of the subgrid viscosity, thus avoiding the use of a subgrid Prandtl number. This subgrid diffusivity, α_{SGS}, expresses as:

$$\alpha_{SGS} = C_\alpha \frac{\bar{\Delta}^2}{\Delta\theta}|\overline{T}|^{\frac{1}{2}}|\Phi_c|^{\frac{1}{4}} \tag{2}$$

In this expression, C_α is a constant taken equal to 0.5 (Sergent et al., 2003) and ($\bar{\Delta}$) is the implicit filter size. $|\overline{T}|$ is an isotropic scalar defined by $|\bar{T}| = \sqrt{2T_{ij}T_{ij}}$, with $T_{ij} = \dfrac{1}{2}(\dfrac{\partial\bar{\theta}}{\partial x_i} + \dfrac{\partial\bar{\theta}}{\partial x_j})\bar{S}_{ij}$, and represents the interactions between the resolved temperature and the resolved velocity field. This first term is built in a similar way than the Smagorinsky model for viscosity. The second term, Φ_c, is homogeneous to a Turbulent Kinetic Energy model and accounts for the thermal heat flux at the cut-off which can be evaluated, following Bardina's similarity scale hypothesis, by explicit filtering of the resolved temperature and velocity fields on a test filter ($\tilde{\bar{\Delta}}$): $\Phi_c = \frac{1}{2}\overline{u_i\theta}'\overline{u_i\theta}'$ with $\overline{u_i\theta}' = \overline{u_i}\,\bar{\theta} - \widetilde{\bar{u}_i}\,\tilde{\bar{\theta}}$. The introduction of the heat flux energy at the cut-off in the modeling allows the subgrid diffusivity to vanish at solid walls or when the heat flux field is fully resolved. This model was successfully applied to different natural convection problems (Sergent et al., 2003; Salat et al., 2004; Sergent et al., 2006).

The LES code is based on the same time marching procedure as the DNS code uses (Sergent et al., 2010).

A finite-volume discretization on staggered grids is used. All the terms involved in the conservation equations are evaluated with a second-order central-differencing scheme, except the nonlinear terms of momentum equations to which a QUICK scheme is applied. The discrete systems resulting from the finite-volume approach are solved by an incremental splitting technique, and the Poisson equation for pressure correction is solved by a direct method using partial diagonalization of the discrete operators of second derivatives.

QUICK scheme has been chosen to improve numerical stability. It is also substantiated by an *a priori* test which had been carried out in the case of the 2D differentially heated cavity at Rayleigh number $Ra = 5 \times 10^{10}$ (Sergent et al., 2003). It has been shown therein that the numerical dissipation of QUICK scheme was able to correctly reproduce the energy transfer between resolved and unresolved flow scales. To summarize, the Mixed Scale Diffusivity Model (MSDM) is used in the energy equation, while no explicit subgrid viscosity model is introduced for the momentum equation.

Note that the use of an upwind correction is consistent with recent observations of Baraghi and Davidson (2007), who mentioned unphysical numerical fluctuations in the transitional vertical boundary layers when central-differencing scheme is used with typical LES mesh resolution.

Grid points are distributed through a hyperbolic distribution in the x direction:

$$x_i = \left(1 + \frac{tanh(\alpha(i/N_x - 0.5))}{tanh(\alpha/2)}\right) \times \frac{A_x}{2} \quad ; \quad 1 \le i \le N_x$$

with $\alpha = 6.81$, as is suggested by Henkes and Hoogendoorn (1992). A smooth hyperbolic distribution ($\alpha = 2$) is considered in the vertical z direction, and a cosine distribution in y direction.

In terms of wall units at $Ra = 1.5 \times 10^9$, the LES grid results in $x^+ \le 0.6$, $\Delta y^+_{max} \le 28$, $\Delta z^+_{max} \le 17$ in the IRC (see next section for case definition).

4 Effects of the front and rear walls

This section is aimed at revealing the effects of the end walls ($y = 0$ and $y = A_y$) on flow structure in the cavity and explaining why the thermal boundary conditions on the front and rear walls are of ultimate importance and how they modify flow structure and the corresponding thermal stratification. For this purpose, appropriate configurations to be investigated are defined first. Validation of LES approach is then followed by end wall effects, comparative analysis with experimental results and discussions.

4.1 Investigated configurations

The previous results (Sergent et al., 2010) have shown that going from PAC to IRC has a substantial influence on the flow structure and on the turbulence level within the cavity. But it has almost no effect on the thermal stratification in the cavity core. Therefore IRC is not the appropriate model of the experimental configuration and the evident drawback of IRC is the adiabatic boundary conditions used on the front/rear walls. In order to understand the end wall effects and have a better agreement between numerical and experimental results, new ingredients are brought in: it is proposed to drop in numerical studies the end walls ($y = 0$ and $y = A_y$) and use periodic conditions on the one hand and to use measured temperature distributions on the front and rear walls and introduce them in 3D numerical simulations as Dirichlet BC on the other hand. Obviously this avoids considering numerically the full thermal coupling of conductive, convective and radiative effects.

The investigated configurations are the following:

- An **Intermediate Realistic Cavity (IRC)** which has been defined (Sergent et al., 2010) has two opposite vertical active walls and adiabatic front and rear walls. On its top and bottom walls, temperature distributions measured along the centerline at $y = A_y/2$ are introduced as thermal BC on the top and bottom walls. This supposes that temperature distributions on these walls are independent of y and t. The experimental measurements of temperature at the centerline on the floor and the ceiling correspond to the following analytical fits (Salat, 2004):

9

$$\begin{cases} \theta_{bottom}(x,y) = (0.5 - x) + 0.994 \dfrac{x(x-1)(x-0.681)}{x(x-1) - 0.0406(x+0.5)} \\ \theta_{top}(x,y) \quad = -\theta_{bottom}(1-x,y) \end{cases}$$

- A **Periodic Realistic Cavity (PRC)** differs from an IRC only in the y spanwise BC. Instead of considering end walls, it is assumed that the solution is periodic in y direction, both for the velocity field and temperature. This configuration is used not only to reproduce flows in the vertical plane at $y = A_y/2$ or in a slab around this vertical plane but also to understand the role played by these walls. In the present study, it represents flows in the shallow cavity central part due to small spanwise aspect ratio ($A_y = 0.32$) while in the experiment of Tian and Karayiannis (2000) where $A_y = 2$, it could represent flows in a larger central part.
- A **Fully Realistic Cavity (FRC)** differs also from an IRC/a PRC only in the thermal BC on the front and rear walls: instead of adiabatic/periodic conditions, thermal BC of Dirichlet type, *ie* measured temperature distributions, are imposed on these walls. In time-averaged sense, flow in the cavity is symmetric with respect to the median vertical plane at $y = A_y/2$. Thus the same temperature distribution is applied to both the front and rear walls. The temperature field on the front wall has been measured by infrared camera and reconstructed analytically (Figure 1). The corresponding time-independent fits (Salat, 2004) are:

$$\theta_1(x,z) = 0.5 - x + \frac{x(x-1)(-8.512 + x(2.65 - 1.5z) + 15.70z - 7.539z^2)}{(x - 1.01)(0.01 + x)(0.85 + 0.5z)} \quad ; z \geq 0.9$$

$$\theta_2(x,z) = 0.5 - x + \frac{0.7692x(x-1)(-0.8528 + 1.3x + 0.4057z)}{(x - 1.01)(0.01 + x)} \quad ; 0.1 < z < 0.9$$

$$\theta_3(x,z) = \theta_1(1 - x, 1 - z) \quad ; z \leq 0.1$$

Using only DNS to investigate these configurations would not have been feasible, because DNS making use of spectral methods requires much larger spatial resolution as well as smaller time steps, and thus much more computational resources, as detailed in Sergent et al. (2010). The above configurations have been studied by means of LES. The numerical parameters for the simulations are reported in Table 1.

	Cavity type	Spatial resolution	Time step	Integ. time	Av. time
LES_{IRC}	Intermediate Realistic	$64 \times 32 \times 128$	0.008	800	320
LES_{PRC}	Periodic Realistic	$64 \times 32 \times 128$	0.008	800	320
LES_{FRC}	Full Realistic	$64 \times 32 \times 128$	0.008	800	320

Table 1
Numerical characteristics for IRC, PRC and FRC.

4.2   Validation of LES methodology: IRC case

LES approaches have been largely used to study turbulent natural convection flows in cavities (Peng and Davidson, 2001; Sergent et al., 2003; Kenjeres et al., 2005; Knopp et al., 2005; Baraghi and Davidson, 2007; Choi and Kim, 2008), it may not be necessary to validate LES methodology in the present work. As comparative analysis in validation procedure can reveal both the capacities and shortcomings of the LES methodology used and our aim is to show by means of LES the reasons of the discrepancy between the numerical results and experimental measurements, it becomes particularly important to do the validation excercise which will especially allow in the following to discriminate the potential weaknesses of the modelling due to the numerical modelling from those pertaining to the physics taken into account in the equations.

It is important to note that both PAC and IRC have been studied by DNS approaches using spectral methods and that reference numerical results are available for the purpose of validation excercise. As is shown previously (Sergent et al., 2010) that the IRC provides the best similarity of flow structure with experiments, it is the IRC configuration that is retained for validating our LES methodology.

In Table 3 are displayed LES results of time-averaged velocity field (various maxima and their positions). In comparison with Table 3 in Part I (Sergent et al., 2010), the largest error observed in the prediction of velocity maxima is inferior to 8% and the locations of these extrema are well reproduced considering the physical problem symmetries and the grid differences. This implies a good agreement between DNS and LES approaches concerning the time-averaged profiles in the mid-depth plane, as it can be seen in Figures 2 and 3. The maximum error on the time-averaged temperature is less than 5%. However the peak of time-averaged velocity is overestimated by LES in the downstream part of the vertical boundary layers as well as in the horizontal boundary layers.
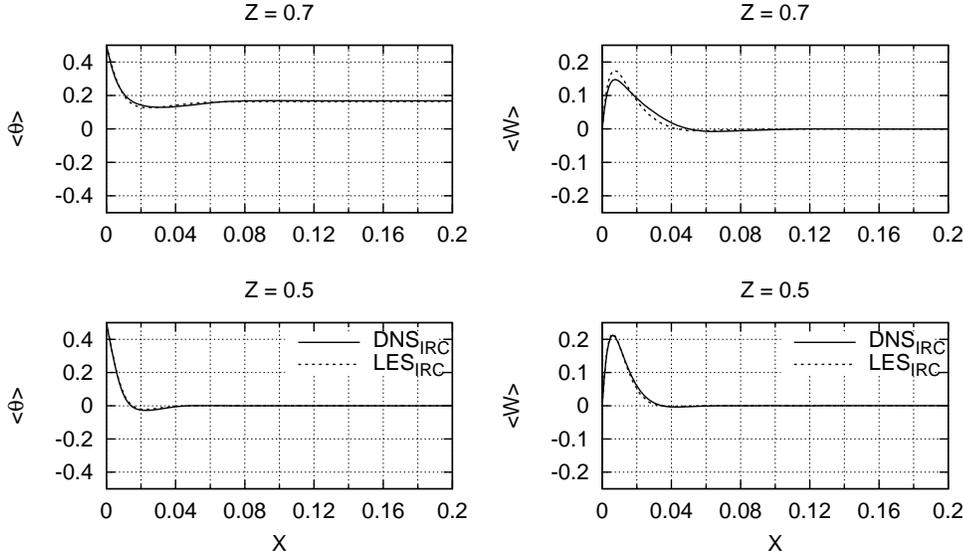
Fig. 2. Horizontal profiles of the time-averaged temperature ($< \theta >$) and vertical velocity ($< W >$) at $y = A_y/2$ and two different heights in the IRC case. Comparison between DNS and LES.

This is the reason why the LES $< Nu_{1D,hot} >$ profile (Figurer 6) displays a laminar shape, whereas the DNS profile exhibits the classical local increase due to the turbulent transition. But the global heat transfer $< \overline{Nu}_{2D,hot-cold} >$ (Table 2) is nonetheless underestimated only with an error smaller than 1% by LES (see also Table 2 in part I for comparison).

With regard to turbulent profiles in the mid-depth plane (Figures 5 and 4), agreement is also good. Temperature and velocity *rms* fluctuations are slightly overestimated in the horizontal boundary layers, but note that θ_{rms} peak values are around 15% lower than the DNS reference in the vertical boundary layers.

Given the good agreement observed between DNS and LES results, our LES methodology is validated in the IRC case and can be thus applied with confidence to the PRC and FRC configurations in order to understand end wall effects and discover the physical phenomena responsible for the weak thermal stratification in experimental studies.

4.3   End walls effects

In order to emphasize the influence of end walls thermal BC on the flow structure, the peculiarity level of the thermal BC is gradually increased
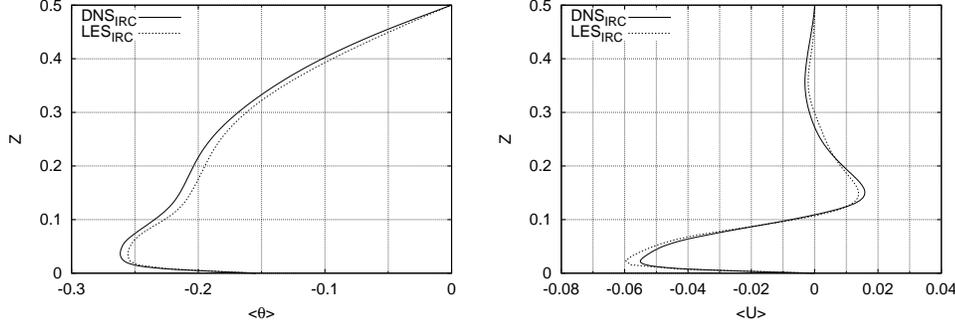
Fig. 3. Vertical profiles of the time-averaged temperature ($< \theta >$) and the horizontal velocity ($< U >$) along the vertical centerline $(x, y) = (A_x/2, y = A_y/2)$ in the IRC case. Comparison between DNS and LES.
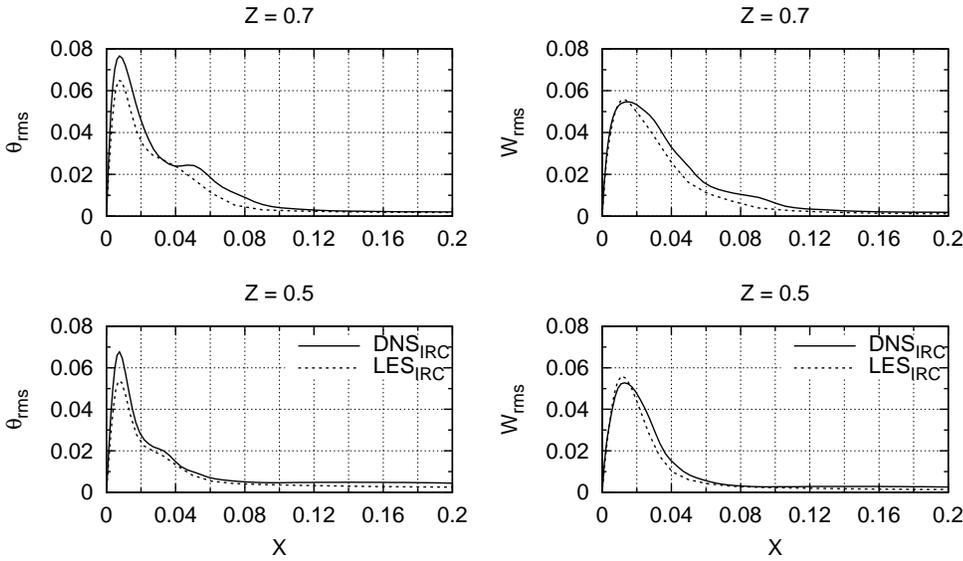

Fig. 4. Horizontal profiles of the *rms* fluctuations of temperature (θ_{rms}) and vertical velocity (W_{rms}) at $y = A_y/2$ and two different heights in the IRC case. Comparison between DNS and LES.

up to integrate the measured temperature in the LES code.

First the PRC configuration is considered. Despite the small cavity depth ($A_y = 0.32$), periodic boundary conditions in y direction do not significantly modify the flow structure which is observed in an IRC. The mean flow in the mid-width vertical plane is shown in Figure 7 for both the IRC and PRC cases: apart from region near the front and rear walls, the time-averaged PRC flow corresponds to the IRC one, and more specifically to the one in the mid-depth plane. This is in good agreement with the observations of Penot and N'Dame (1992), who have shown that shallow cavities are slightly affected by 3D effects. This minor change in the
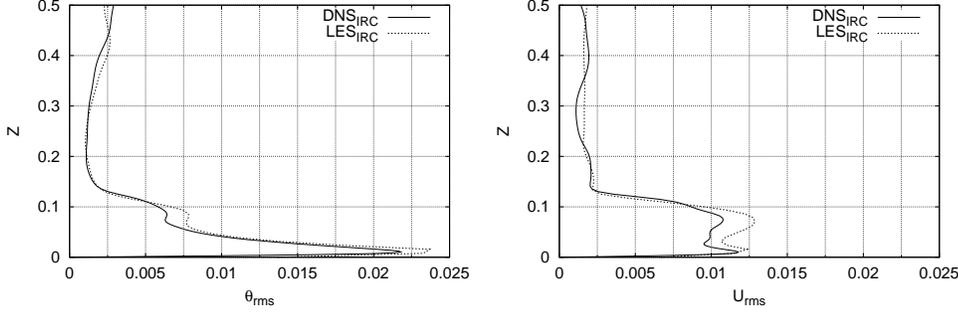
Fig. 5. Vertical profiles of the *rms* fluctuations of temperature (θ_{rms}) and vertical velocity (U_{rms}) along the vertical centerline $(x, y) = (A_x/2, y = A_y/2)$ in the IRC case. Comparison between DNS and LES.
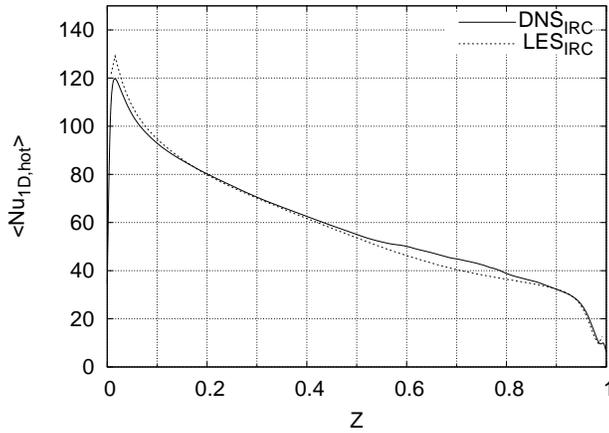

Fig. 6. Vertical profile of the time-averaged Nusselt number along the hot wall in the mid-depth plane $(y = A_y/2)$ in the IRC case. Comparison between DNS and LES.

flow has no influence on the thermal field and the thermal stratification keeps a value equal to 1 (table 2). This has also been observed by Trias et al. (2007) and Trias et al. (2010) in a 3D cavity of aspect ratio 4 with periodic BC in the spanwise direction. It means that the thermal boundary conditions applied in an IRC/a PRC allow to simulate basically the experimental flow structure of the global peripheral circulation, as it has been described from the DNS data in the first part of this paper (Sergent et al., 2010). Nonetheless these configurations do not allow to reproduce the physical phenomena occurring in the cavity center, and particularly the thermal stratification. This finding contradicts the results of Peng and Davidson (2001). In their study, LES performed on PRC and IRC configurations led to a thermal stratification equal to about 0.5, which is close to the experimental results of Tian and Karayiannis (2000). The reason why such a value has been obtained is discussed in section 4.5.

	S	$< \overline{Nu}_{1D,hot-cold} >$	$< \overline{Nu}_{2D,hot-cold} >$	$< \overline{Nu}_{1D,bot-top} >$	$< \overline{Nu}_{2D,bot-top} >$
LES_{IRC}	1.	58.7	57.3	13.5	13.0
LES_{PRC}	1.	58.2	58.2	12.3	12.3
LES_{FRC}	0.42	55.3	54.3	10.6	10.0
EXP	0.375	55.4 (hot wall)	not measured	6.1 (bottom wall)	not measured
		54.2 (cold wall)	not measured	6.5 (top wall)	not measured

Table 2
Time-averaged thermal stratification S and Nusselt numbers at wall for IRC,
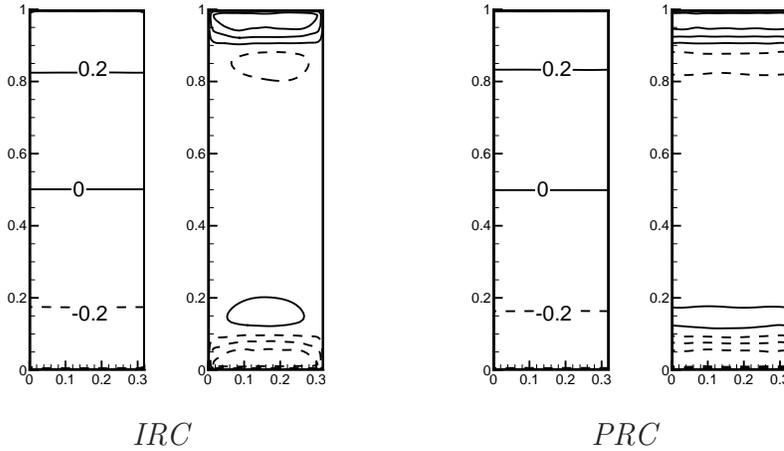PRC and FRC cases and experiment.

IRC   PRC

Fig. 7. Isocontours of temperature $< \theta >$ and horizontal velocities
($< U >= [\pm0.05; \pm0.03; \pm0.01]$) at the vertical mid-width plane ($x = A_x/2$).
Comparison between IRC (left) and FRC (right).

Although comparison between IRC and PRC did not show any improve-
ment in predicting thermal stratification in the cavity core, it does show
that periodic and adiabatic thermal boundary conditions are very simi-
lar and that in an IRC the only effect of the end walls is on flow struc-
ture and due to the no-slip condition. This leads to the conclusion that
the difference between numerically investigated IRC configuration and
experimentally studied cavity must come from the thermal boundary
condition—the adiabatic condition on the front/rear walls. The last way
to obtain an agreement between numerical and experimental approaches
is to use measured temperature distribution as thermal boundary condi-
tions on the end walls, ie to study numerically the FRC configuration.

In comparison with the IRC configuration, LES performed on FRC con-
figuration indicates only a slight modification in terms of velocity maxima
(Table 3) except for the horizontal velocity component ($< U >$): the in-

crease is noticeable in the cavity corner upstream from the horizontal boundary layers Heat transfer on the two isothermal walls is slightly reduced in FRC in comparison with IRC (table 2). However inspection of time-averaged flow structure (Figure 8) shows a clear modification: despite the fact that main flow features (the peripheral clockwise circulation, the two horizontal flow reversals, the reflexion symmetry about the mid-depth plane at $y = A_y/2$ and the 2D centro-symmetry) remain the same, in the FRC case the horizontal flow reversals are stronger and time-averaged flow is more three-dimensionnal near the front and rear walls.

Figures 9 and 10 indicate clearly the changes that took place for time-averaged velocity ($< V >$ and $< W >$) and temperature fields. In the mid-depth vertical plane, time-averaged temperature field shows a weak vertical gradiant on the one hand and on the other hand the thermal boundary condition applied on the front and rear walls in the FRC case induces a secondary flow near these walls. In fact, Figure 11), displaying time-averaged isotherms and streamlines in a vertical plane near the front wall, shows that streamlines are mainly normal to the horizontal isotherms and that they converge vertically to a line at which the fluid is redirected horizontally toward the cavity mid-depth (see also Figure 8). In order to exhibit the flow structure in the cavity core, Figure 12 displays time-averaged streamlines in the three middle planes at respectively $x = A_x/2$, $y = A_y/2$ and $z = 1/2$. The cavity core is no more nearly stagnant as in IRC, but crossed by a weak horizontal flow: at the mid-width ($x = A_x/2$) time-averaged flow converges horizontally to the mid-depth, at the mid-depth ($y = A_y$) it diverges horizontally from the mid-with to respectively the hot and cold walls while at the mid-heihgt ($z = 1/2$) it starts from the front and rear walls and ends up to respectively the hot wall for $x < A_x/2$ and the cold wall for $x > A_x/2$. This draws the following picture: near the top wall, part of hot fluid leaves the main stream and moves downwards along the end walls before being redirected to the cavity core at a particular vertical position; depending on the redirected position, fluid particules will join either the hot wall or the cold wall. The same arguments stand for cold fluid near the bottom wall.

In terms of thermal stratification in the cavity core, the resulting vertical temperature grdient is $<S>= 0.42$ (Table 2) qui is in fact close to the vertical temperature gradient ($\partial\theta_2/\partial z(A_x/2, 0.5) \sim 0.3$) of the thermal BC (Eq. 3) applied on the front/rear walls. It means that the thermal BC used in the FRC configuration, ie the measured temperature, are essential and responsible for the weak thermal stratification. In order to emphasize these effects, another FRC configuration with simpler thermal BC on the

16

LES$_{IRC}$			LES$_{FRC}$		
$< U >_{max}$	$< V >_{max}$	$< W >_{max}$	$< U >_{max}$	$< V >_{max}$	$< W >_{max}$
Maxima of velocity components on the entire volume					
0.1196	0.0292	0.2488	0.1597	0.0272	0.2462
$x = 0.0742$	0.0267	0.0069	$x = 0.0742$	0.0267	0.0069
$y = 0.2736$	0.3113	0.3049	$y = 0.0463$	0.3113	0.0150
$z = 0.9922$	0.9922	0.5000	$z = 0.9922$	0.9922	0.6484
Maxima of velocity components on the mid-depth plane, $y = A_y/2$					
0.1161	0.0030	0.2211	0.1531	0.0059	0.2155
$x = 0.0742$	0.0902	0.0054	$x = 0.0742$	0.0609	0.0069
$z = 0.9922$	0.9531	0.4453	$z = 0.9922$	0.8828	0.6406
Maxima of velocity components on the mid-height plane, $z = A_z/2$					
0.0048	0.0039	0.2487	0.0015	0.0028	0.2439
$x = 0.0329$	0.0173	0.0069	$x = 0.0267$	0.0017	0.0069
$y = 0.0086$	0.2736	0.3049	$y = 0.311$	0.3049	0.0086

Table 3

Maxima of the time-averaged velocity components for IRC and FRC cases.

front and rear walls has been investigated: the front and rear walls are supposed to be isothermal at $\theta = 0$. Similar flow structure is observed, but note that near the front and rear walls time-averaged flow converges at the cavity mid-height and that flow reversals are stronger. This results in a stratified cavity core limited to one fifth of the cavity height with a central stratification equal to 0.06. It confirms therefore that temperature distributions on the end walls are the key factor explaining the weak thermal stratification in the cavity core. The question thatreamins to be answered is then from where these temperature distributions responsible for the weak thermal stratification come.

4.4 Comparison with experimental results

Des modifs sont faites dans cette subsection.

In order to show that using measured temperature distributions as Dirichlet boundary condition on the front and rear walls improves numerical
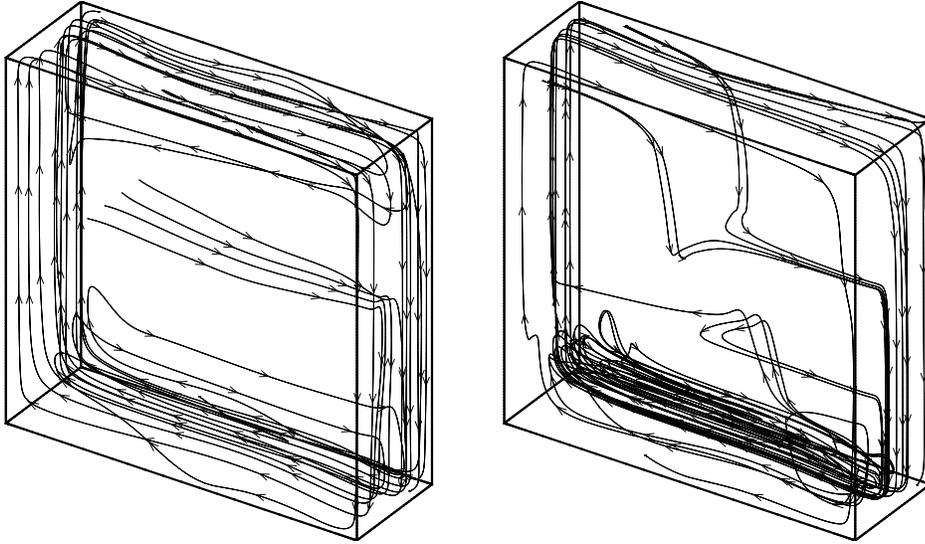
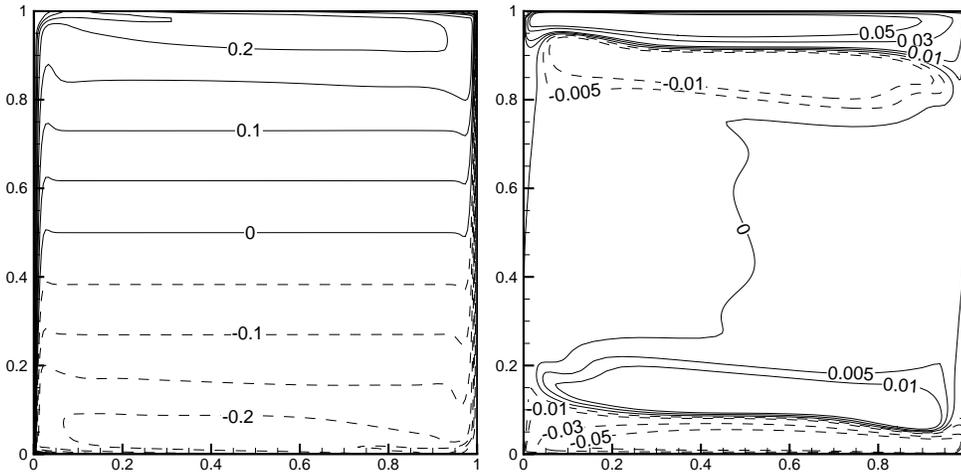Fig. 8. Streamlines in the time-averaged flow for IRC (left) and FRC (right).

Fig. 9. Isocontours of temperature $< \theta >$ (left) and horizontal velocity $< U >$ (right) in the vertical mid-depth plane ($y = A_y/2$) in the FRC.

prediction, LES results of the FRC are compared briefly with experimental measurements (Salat, 2004). The comparison is focused on the vertical profiles of temperature and velocity because they are the most difficult to be accurately repoduced in numerical simulations as has been shown before. A more detailed comparison is made in the third part of this paper (Xin et al., 2010).

Figure 13 shows clearly that the agreement between experiment and simulation is better with the FRC than with IRC. The vertical time-averaged profiles of horizontal velocity component ($< U >$) and temperature are

18

IRC   FRC
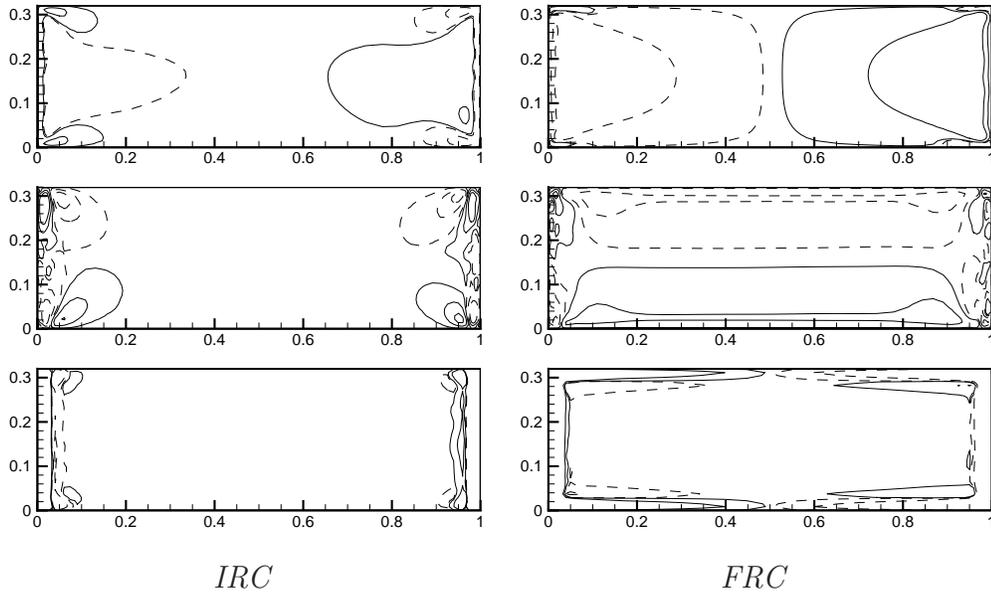
Fig. 10. Isocontours of velocity components in the horizontal mid-height plane ($z = A_z/2$). From top to bottom, horizontal velocity ($< U > = [\pm 0.0002; \pm 0.002]$), spanwise velocity ($< V > = [\pm 0.0002; \pm 0.001; \pm 0.002]$) and vertical velocity ($< W > = [\pm 0.0002; \pm 0.002]$). Comparison between IRC (left) and FRC (right).
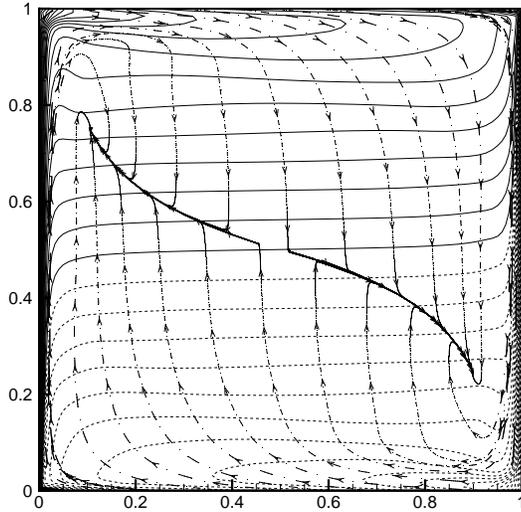

Fig. 11. Superimposition of the isocontours of temperature $< \theta >$ and streamlines in the time-averaged flow on the vertical plane close to the front wall ($y = 0.00866$) for the FRC cavity.
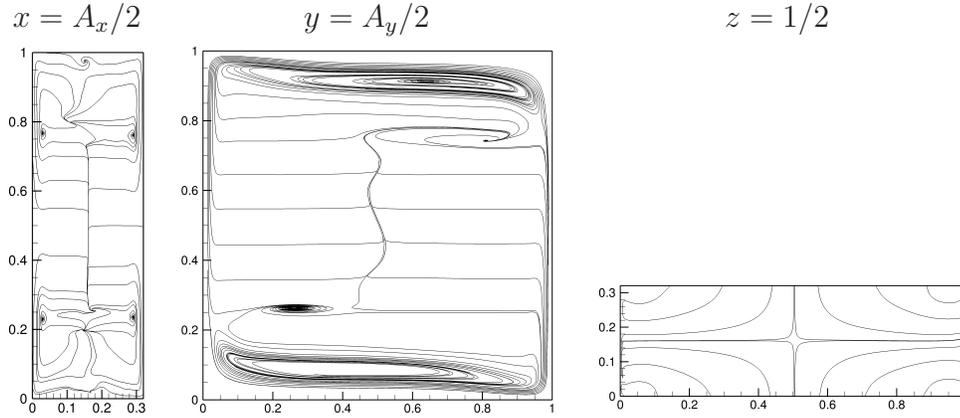
$x = A_x/2$ $y = A_y/2$ $z = 1/2$

Fig. 12. Projections of FRC time-averaged streamlines on the three median planes.

in good agreement with the experimental data, particularly in the cavity core for $0.3 \leq z \leq 0.7$. Noteworthy is the improvement in the thermal stratification ($<S>$) estimation: even though $<S>_{FRC}$ ($= 0.42$) is slightly higher than the experimental value $<S>_{EXP}$ ($= 0.375$), it is much lower than $<S>_{IRC}$ ($= 1$) (see Table 2). However differences still persist in the horizontal boundary layers. The horizontal flow pertaining to the general clockwise circulation is overestimated by LES and so for the peak value of temperature. The resulting $< \overline{Nu}_{1D,bottom-top} >$ is also overestimated in comparison with the experimental data (see Table 2). Concerning the rms fluctuations, the order of magnitude of the FRC and experimental results are similar. The slight FRC over-prediction may stem from the LES models, as will be explained in section 4.2.

It is clear that temperature distributions imposed on the four passive walls manifest a significant influence on the flow global organization. They contribute to an appreciable improvement in numerical prediction of the flow structure when experimental thermal measurements are used in the numerical code. Note however that there are slight discrepancies between measured temperature distributions and the fitted expressions and that they may induce substantial differences between numerical and experimental results, especially in the cavity core. J'ai commenté la phrase sur le coupage : S'il faut la remettre, on doit enlever la phrase sur les mesures et les fits.
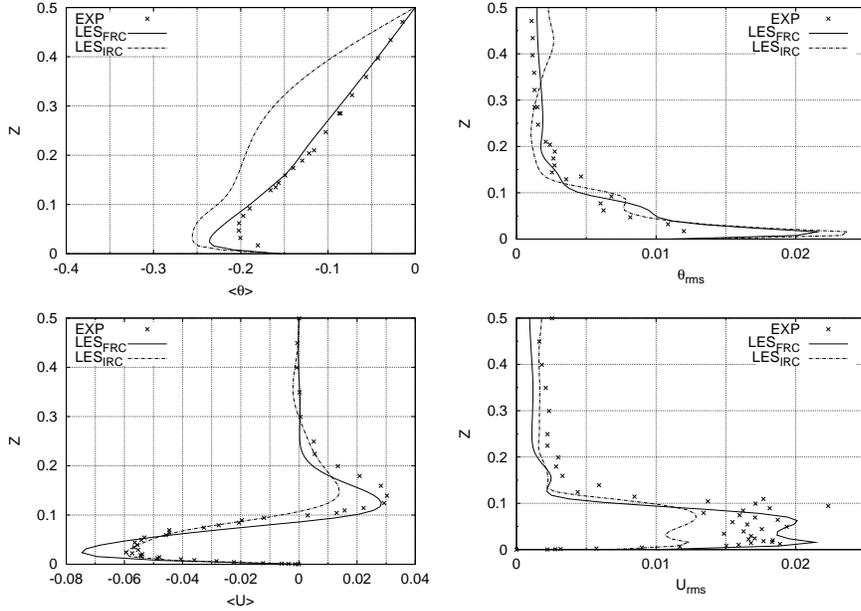
Fig. 13. Vertical profiles along the centerline $(x, y) = (A_x/2, A_y/2)$ of the time-averaged temperature $(< \theta >)$, the horizontal velocity $(< U >)$ and their respective *rms* fluctuations (left). Comparison between FRC results and experimental data.

4.5 Discussion

In order to remove any ambiguity, spectral DNS in the *IRC* configuration have been presented (Sergent et al., 2010). It has come as an evidence that introducing the experimental temperature distributions along the top and bottom walls is not sufficient to predict correctly the measurements, especially the low experimental thermal stratification in the cavity core.

Up to now, two physical mechanisms may be put forward to explain the low stratification of the air-filled cavity core: (i) the turbulent transition of the vertical boundary layers or (ii) the radiative heat transfer.

(i) It is usual to consider that the turbulent transition of the vertical boundary layers is responsible for the strengthening of the vortex ejection leading to a stratification increase. It has recently been observed numerically (Trias et al., 2010) in an air-filled adiabatic-periodic configuration. The question of the low experimental stratification may be also interpreted as a particular case where a very early destabilization of the vertical boundary layers may destroy the central stratification.

(ii) The present work shows in contrary that the front and rear walls temperature distributions create a weak but 3D flow carrying fluid from

the horizontal clockwise main stream to the end walls first, then the cavity core and finally the vertical main stream (either the hot or the cold walls) and reducing the cavity core stratification.

As at $Ra = 1.5 \times 10^9$ the transition point is above $z = 0.5$, it can be concluded that turbulent transition is not the relevant mechanism, that what happens near the front and rear walls is responsible for the low thermal stratification and that the end walls are far from being convectively adiabatic.

Along with this conclusion comes the question of the validity of the simulations presented in Peng and Davidson (2001). In these simulations performed at $Ra = 1.58 \times 10^9$, experimental temperature measurements taken from Tian and Karayiannis (2000) have been applied to top and bottom walls whereas adiabaticity has been imposed at the end walls. A good agreement between experimental and numerical results has been obtained especially concerning the temperature field. Given the fact that convectively adiabatic conditions do not coorespond to what happens physically in the experimental set-up, the good agreement between the experiment of Tian and Karayiannis (2000) and the numerical simulations of Peng and Davidson (2001) that there should not be would result from a numerical artefact, related to numerical scheme and/or turbulence modelling. Indeed both of them can be responsible for numerical instabilities in the vertical boundary layers as mentionned by Baraghi and Davidson (2007). A numerical destabilization of the vertical boundary layers would explain the low thermal stratification observed.

The present work established that the front and rear walls do not follow a simple convective adiabaticity. But which kind of thermal conditions there should be on the end walls in the experiments of Salat (2004) and Tian and Karayiannis (2000) and where they come from remain to be answered. The effects of a radiatively participating medium have been studied by Borjini et al. (2008) in a differentially heated cavity filled with a large Prandtl number fluid ($Pr = 13.6$) at $Ra = 10^5$, where spiraling flows take place. An important effect of the radiative transfer on the flow structure has been observed in the cavity core whereas the peripheral spiral flow is not affected. The recurrently observed discrepancies between numerical and experimental results in air-filled cavities, particularly on the thermal stratification, can come from a complete thermal balance at the cavity walls, including conductive and radiative transfer. As air is likely a transparent medium, the corresponding radiative transfer would appear in the simplest form: surface radiation.

This supposes that, at least in an air-filled cavity, recovering of the experimental results can not be obtained without considering explicitly or implicitly (Dirichlet BC) a complete radiation-convection-conduction coupling between cavity walls and fluid. As implicit consideration of the full coupling through Dirichlet BC relies heavily on experimental works, explicit coupling will be investigated in the third part of this paper.

5   Conclusion

In Part I of the present paper (Sergent et al., 2010), it has been concluded that considering measured temperature distributions only on the horizontal walls in 3D spectral DNS, *ie* studying numerically an intermediate realistic cavity (IRC), is not sufficient to reproduce the experimentally observed thermal stratification. The global flow characteristics in the boundary layers of the IRC are however close to the experimental observations. Accordingly the IRC configuration has been retained in Part II for validating our LES methodology, whose results have been proved to be in good agreement with the DNS data.

A particular attention has been paid to the effect of the thermal BC applied on the front and rear walls. Two additional configurations, a periodic realistic cavity (PRC) and a fully realistic cavity (FRC), have been defined and studied by LES approach. When using periodic conditions in y direction in a PRC, time-averaged temperature is almost the same as in an IRC and time-averaged velocity field in the cavity keeps the main flow features in an IRC except for in regions near the end walls. The only difference between the IRC and PRC configurations is due to the no-slip condition applied on the front and rear walls. It is concluded therefore that the thermal boundary condition—the convectively adiabatic condition on the front/rear walls is the only factor responsible for the difference between numerically investigated IRC configuration and experimentally studied cavity. This leads naturally to the conclusion that the front and rear walls in the experiments of are not convectively adiabatic on the one hand and on the other hand the idea that one has to introduce the experimental temperature distributions on the front and rear walls in numerical simulations, *ie*, study the FRC configuration. LES has been performed for the FRC configuration and the corresponding results are in very good agreement with the experimental data, particularly in terms of the thermal stratification in the cavity core. The good agreement between LES results in a FRC and experimal data proves that the front and rear walls do not simply act as convectively passive walls: they are

active in terms of heat transfer and fluid flow. As weak thermal stratification observed in experiments comes mainly from 'active' front and rear walls, the major conclusion of Part II is that any numerical simulations using adiabatic end walls should never recover experimentally observed thermal stratification.

As discussed above, 'active' front and rear walls can be due to radiative, conductive and convective coupling that takes place on these walls. From a numerical point of view, this coupling can be considered either by introducing a complete set of thermal BC, as presented in this paper, or by introducing explicitly surface radiation and heat conduction in cavity walls. In the former, preliminary experiments need to be done before computations, while in the latter the knowledge of materials physical properties is only required. Such a complete coupling between surface radiation, conduction in the walls and convection is developed in the third part of this paper (Xin et al., 2010) with a pseudo-spectral approach, in order to identify the role played by each transfer mode and explain the temperature distributions observed on the different walls.

References

Ampofo, F., Karayiannis, T. G., 2003. Experimental benchmark data for turbulent natural convection in an air filled square cavity. International Journal of Heat and Mass Transfer 46 (19), 3551 – 3572.

Baraghi, D. G., Davidson, L., 2007. Natural convection boundary layer in a 5:1 cavity. Phys. Fluids 19, 1–15.

Betts, P. L., Bokhari, I. H., 2000. Experiments on turbulent natural convection in an enclosed tall cavity. International Journal of Heat and Fluid Flow 21 (6), 675 – 683.

Borjini, M., Aissia, H. B., Halouani, K., Zeghmati, B., 2008. Effect of

radiative heat transfer on the three-dimensional bouyancy flow in cubic enclosure heated from the side. Int. J. Heat Fluid Flow 29, 107–118.

Cheesewright, R., King, K., Ziai, S., 1986. Experimental data for the validation of computer codes for the prediction of two-dimensional buoyant cavity flows. In: Notes on Numerical Flow Dynamics. Vol. 60 of ASME Winter Annual Meeting. pp. 75–81.

Choi, S.-K., Kim, S.-O., 2008. Treatment of turbulent heat fluxes with the elliptic-blending second-moment closure for turbulent natural convection flows. International Journal of Heat and Mass Transfer 51 (9-10), 2377 – 2388.

Feldman, Y., Gelfgat, A. Y., 2009. On pressure-velocity coupled time-integration of incompressible navier-stokes equations using direct inversion of stokes operator or accelerated multigrid technique. Comput. Structures 87 (11-12), 710 – 720, fifth MIT Conference on Computational Fluid and Solid Mechanics.

Fusegi, T., Hyun, J. M., 1994. Laminar and transitional natural convection in an enclosure with complex and realistic conditions. International Journal of Heat and Fluid Flow 15 (4), 258 – 268.

Henkes, R. A. W. M., Hoogendoorn, C. J., 1992. Turbulent natural convection in enclosures; a computational and experimental benchmark study. Proc. ERCOFTAC/EUROTHERM Sem. 22, Delft. EETI, Paris.

Kenjeres, S., Gunarjo, S., Hanjalic, K., 2005. Contribution to elliptic relaxation modelling of turbulent natural and mixed convection. International Journal of Heat and Fluid Flow 26 (4), 569 – 586, cHT'04.

Knopp, T., Lube, G., Gritzki, R., Rösler, M., 2005. A near-wall strategy for buoyancy-affected turbulent flows using stabilized fem with applications to indoor air flow simulation. Computer Methods in Applied Mechanics and Engineering 194 (36-38), 3797 – 3816.

Le Quéré, P., 1994. Onset of unsteadiness routes to chaos and simulations of chaotic flows in cavities heated from the side: a review of present status. Vol. 1 of 10th Int. Heat Transfer Conf., Brighton, UK. pp. 281–296.

Mergui, S., Penot, F., 1997. Analyse des vitesse et température de l'air en convection naturelle dans une cavité carrée différentiellement chauffée à $Ra = 1.69 \times 10^9$. Int. J. Heat Mass Transfer 40, 3427–3441.

Peng, S., Davidson, L., 2001. Large eddy simulation for turbulent buoyant flow in a confined cavity. Int. J. Heat Fluid Flow 22, 323–331.

Penot, F., N'Dame, A., 1992. Successive bifurcations of natural convection in a vertical enclosure heated from the side. Vol. 1 of 1st European thermal-sciences and 3rd UK national heat transfer conference, Birmingham. pp. 507–514.

Sagaut, P., 1996. Numerical simulations of separated flows with subgrid

models. Rech. Aérospatiale (english version) 1, 51–63.

Salat, J., 2004. Contribution à l'étude de la convection naturelle tridimensionnelle en cavité différentiellement chauffée. Ph.D. thesis, Université de Poitiers.

Salat, J., Penot, F., 2003. Approche expérimentale de la convection naturelle en transition turbulente dans une cavité cubique différentiellement chauffée. VIe Colloque Interuniversitaire Franco-Québecois de Thermique des Systèmes, 26-28 mai 2003, Québec. pp. 75–81.

Salat, J., Xin, S., Joubert, P., Sergent, A., Penot, F., Le Quéré, P., 2004. Experimental and numerical investigation of turbulent natural convection in a large air-filled cavity. Int. J. Heat Fluid Flow 25 (5), 824–832.

Sergent, A., Joubert, P., Le Quéré, P., 2003. Development of a local subgrid diffusivity model for large eddy simulation of buoyancy driven flows: application to a square differentially heated cavity. Num. Heat Transfer Part. A 44 (8), 789–810.

Sergent, A., Joubert, P., Le Quéré, P., 2006. Large eddy simulation of turbulent thermal convection using a mixed scale diffusivity model. Prog. Comp. Fluid Dynamics 6 (1/2/3), 40–49.

Sergent, A., Xin, S., Joubert, P., Le Quéré, P., Salat, J., Penot, F., 2010. Resolving the stratification discrepancy of turbulent natural convection in differentially heated air-filled cavities. part i: Reference solutions. Int. J. Heat Fluid Flow , submitted.

Tian, Y., Karayiannis, T., 2000. Low turbulence natural convection in an air filled square cavity, part I & II. Int. J. Heat Mass Transfer 43, 849–884.

Trias, X., Gorobets, A., Soria, M., Oliva, A., 2010. Direct numerical simulation of a differentially heated cavity of aspect ratio 4 with Rayleigh numbers up to 10^{11} - part I: Numerical methods and time-averaged flow. Int. J. Heat Mass Transfer 53, 665–673.

Trias, X., Soria, M., Oliva, A., Pérez-Ségarra, C. D., 2007. Direct numerical simulation of two and three-dimensional natural convection flows in a differentially heated cavity of aspect ratio 4. J. Fluid Mech. 586, 259–293.

Tric, E., Labrosse, G., Betrouni, M., 2000. A first incursion into the 3d structure of natural convection of air in a differentially heated cubic cavity, from accurate numerical solutions. Int. J. Heat Mass Transfer 43, 4043–4056.

Wakashima, S., Saitoh, T. S., 2004. Benchmark solutions for natural convection in a cubic cavity using the high-order time-space method. International Journal of Heat and Mass Transfer 47 (4), 853 – 864.

Xin, S., Joubert, P., Sergent, A., Le Quéré, P., 2010. Resolving the strat-

ification discrepancy of turbulent natural convection in differentially heated air-filled cavities. Part III: a full convection-conduction-surface radiation coupling. Int. J. Heat Fluid Flow , submitted.